

Depth seismic imaging using reflection and first arrival traveltimes tomography: Application to a deep profile across the Northern Emirates Foothills

Anne Jardin, Karine Broto, and Timothée Perdrizet

Introduction

When geology shows substantial structural complexity, depth migration of time seismic data is required to avoid misleading interpretation errors. This processing however, requires the determination of an accurate depth velocity model (Versteeg 1994). Prestack reflection traveltimes tomography is a well-known approach for building reliable velocity models (Bishop et al. 1985; Jurado et al. 1996). The implementation made at IFP Energies nouvelles of prestack reflection tomography has proven its effectiveness on several real datasets in complex geological settings (Broto and Ehinger 1998; Ehinger et al. 2001; Bêche et al. 2005; Bêche 2009). It was also used to detect strong velocity variations induced by gas presence (Broto et al. 2003; Plaza et al. 2010; Broto et al. 2011). But when seismic reflections become difficult to be identified and picked, this method suffers from severe limitations.

As opposed to depth tomography or migration velocity analysis methods (Stork 1992; Bloor 1998; Gray et al. 2000), traveltimes inversion or tomography may be straightforwardly extended to inversion of any type of seismic events. These inversion processes can be performed sequentially or simultaneously (Broto et al. 2003; Broto and Lailly 2001). This high flexibility of traveltimes tomography makes this technique very attractive when dealing with complex media. Furthermore any available seismic information can be inverted within a single run computing a unified velocity

model of the subsurface. First arrivals or turning rays are commonly inverted by traveltimes tomography to estimate the near surface velocities (Zelt and Barton 1998; Zhu et al. 2000). Methods or workflows combining both reflection and first arrival information are nowadays more and more widely investigated for accessing velocities in such complex context as foothills (Gray et al. 2002; Dell'Aversana et al. 2003; Zhu et al. 2008; Jaiswal and Zelt 2008).

In this study, we propose to simultaneously invert primary reflections and first arrivals in a joint tomographic process. The objective is to benefit from the data density of the first arrivals in the shallower areas and from the depth investigation of reflections in the deepest zones. We firstly describe the joint tomography method and secondly its application on a deep seismic profile acquired through the Northern Emirates foothills. Finally, the contribution of this study to a better recognition of the geological structures is discussed.

Methodology

The Traveltimes Tomographic Inverse Problem

The traveltimes tomographic inversion aims at determining the velocity model that minimizes the misfits between observed traveltimes obtained from interpretation of seismic events and calculated traveltimes computed by seismic ray-tracing. This problem being ill-posed, a priori information about the subsurface model is introduced through a regularization term (Tarantola 1987). As shown by Delprat-Jannaud and Lailly (1993), a priori information on the second derivatives of the model is necessary and sufficient to obtain a mathematically well-posed problem. Hence the general inverse problem of traveltimes tomography can be written as the minimization of the following least-square objective function:

$$C(\mathbf{m}) = \|\mathbf{T}^{cal}(\mathbf{m}) - \mathbf{T}^{obs}\|^2 + \varepsilon_R \|\mathbf{D}^2(\mathbf{m} - \mathbf{m}^{prior})\|^2, \quad (7.1)$$

A. Jardin (✉) · K. Broto
IFP Energies Nouvelles, 1 et 4 Avenue de Bois-Préau, 92 852
Rueil, Malmaison, France
e-mail: anne.Jardin@ifpen.fr

K. Broto
e-mail: karine.Broto@ifpen.fr

T. Perdrizet
IFP Energies Nouvelles, Rond-Point de l'échangeur de Solaize,
BP 3, 69360 Solaize, France
e-mail: timothee.Perdrizet@ifpen.fr

where $\|T^{cal}(\mathbf{m}) - T^{obs}\|^2$ is called the traveltimes term, T^{obs} being the vector of observed traveltimes, $T^{cal}(\mathbf{m})$ containing the calculated traveltimes through the model \mathbf{m} , and $\|D^2(\mathbf{m} - \mathbf{m}^{prior})\|^2$ is the second order regularization term with respect to a priori model \mathbf{m}^{prior} , ϵ_R allowing to weight the regularization term with respect to the traveltimes term.

Equation 7.1 is commonly used to solve the reflection traveltimes tomography problem, i.e. to determine the subsurface model that explains traveltimes resulting from the interpretation of seismic reflections. Equation 7.1 is actually valid for any type of traveltimes information and can also be extended to the joint inversion of different types of traveltimes information within a single simultaneous run.

Considering joint reflection and first arrival tomographic inversion, Eq. 7.1 can be reformulated as the minimization of the following cost function:

$$C(\mathbf{m}) = \epsilon_{RT} \|T_{RT}^{cal}(\mathbf{m}) - T_{RT}^{obs}\|^2 + \epsilon_{FA} \|T_{FA}^{cal}(\mathbf{m}) - T_{FA}^{obs}\|^2 + \epsilon_R \|D^2(\mathbf{m} - \mathbf{m}^{prior})\|^2, \quad (7.2)$$

where RT stands for reflection traveltimes, FA for first arrival traveltimes, ϵ_{RT} and ϵ_{FA} allowing to weight respectively the reflection term and the first arrival term.

Velocity Model Representation

The complexity of the model \mathbf{m} which can be retrieved by tomography depends on the chosen mathematical representation of spatial velocity variations. Two main representations are generally used: the smooth representation, for which the subsurface is represented by a single smoothly varying function and the blocky representation, for which the subsurface is divided into blocks separated by interfaces. We implement a hybrid representation that we call ‘‘a smooth per block representation’’ to benefit from the advantages of both representations (Lailly and Sinoquet 1996). Each block is delimited by interfaces and characterized by its proper smooth velocity distribution which may be constant, laterally varying (type $v(x, y)$), with or without a vertical gradient (type $v(x, y) + kz$, or laterally and vertically varying (type $v(x, y, z)$). We make use of bi-cubic B-spline functions for representing the interfaces and velocity block laws to ensure the continuity of second order derivatives as requested by Eq. 7.1 or 7.2. Compared to a pure smooth representation of the velocity model, this hybrid representation allows to build models with strong velocity contrasts—such as those encountered when crossing faults, salt or basalt bodies—and with smooth velocity variations inside each individual block—such as those induced by facies changes, tectonic stresses, or fluid injection.

Ray-Tracing Modelling

At each step of the iterative inversion process, forward modelling by means of prestack ray-tracing is performed to compute the prestack traveltimes associated with the current velocity model. In the case of reflection traveltimes ($T_{RT}^{cal}(\mathbf{m})$ term in Eq. 7.2), the bending method has been chosen for sake of efficiency (Jurado et al. 1996). In this method, a ray joining a source to a receiver is updated until the total traveltimes is stationary (Fermat’s principle). Circular arcs are used when the velocity is varying with a constant vertical gradient and straight lines otherwise. Ghost interfaces defined as virtual interfaces could be introduced in the blocky model to improve the accuracy of the calculated traveltimes by splitting long rays into smaller segments. Accurate traveltimes are computed with this ray-tracing technique, even through complex structures like triangle zones (Jardin et al. 2005).

In the case of the first arrival traveltimes ($T_{FA}^{cal}(\mathbf{m})$ term in Eq. 7.2), the forward problem is solved by a paraxial ray-tracing for the calculation of the first arrival data, modelled as turning rays or diving rays propagating through a smooth medium (Clarke 1997).

Access to Observed Travel Times

The observed traveltimes T^{obs} in Eq. 7.1 or 7.2 are obtained by picking seismic events in prestack time gathers. Interpreting seismic reflections in prestack data is a tedious task: it means handling, visualizing, understanding and picking a huge amount of data. Furthermore, prestack seismic data are generally characterized by a poor signal-to-noise ratio and seismic events may be distorted and difficult to be clearly identified in the time domain. Finally, because of the inherent move-out of seismic events in the prestack time domain, it may be difficult to ensure the consistency of the interpretation from one common offset section to the next one. The traveltimes database may thus be incomplete or contain important interpretation errors, hence compromising the results of the tomographic inversion (Broto 1999). Original methodologies to ensure that this database is complete and accurate as much as possible have been developed (Grau and Lailly 1993; Broto and Ehinger 1998; Broto et al. 2008). However, human involvement remains important. On the other hand, first arrivals are clearly identifiable in seismic data and industrial software can be used to pick the required first breaks on unmigrated gathers. As for reflection traveltimes, the picking quality of first arrivals can however, be affected by ambient noise. This quality control of reflection and first arrival traveltimes picking will be a factor for defining the relative values of weights ϵ_{RT} and ϵ_{FA} in Eq. 7.2.

Inversion Process

Since the physical law $T^{cal}(m)$ used to estimate calculated data for a given model m is non linear, the cost function described in Eqs. 7.1 and 7.2 is non quadratic. In the implementation of IFPEN's traveltimes tomography software, this non linear problem is solved iteratively with the Gauss–Newton method. Any velocity model determination method is exposed to the non-unicity of the solution. This difficulty derives from the fact that the recorded data are restricted to a limited range of source-receiver offsets and azimuths. As discussed above, the hybrid representation of the subsurface and the introduction of a priori information allow to reduce respectively the number of unknowns of the problem and the solution space. Tuning regularization weights can however be very delicate. To overcome this difficulty, a method has been proposed (Renard et Lailly 1999; Plaza et al. 2010). It consists in starting the inversion with strong regularization weights, then in regularly decreasing these weights to derive models that are less and less smooth. This process is stopped when traveltimes misfits do no longer decrease. In addition to the regularization of the inverse problem, our implementation of traveltimes tomography can account for hard constraints on the searched model (Delbos et al. 2006). These inequality or equality constraints may correspond to geological or geophysical knowledge, such as the range of expected velocity values, expected interface depths, expected dips or roughness etc.

Application to a Deep Seismic Profile

The Oman range and Northern Emirates Foothills have been studied by geologists for a long time but mainly in the Sultanate of Oman. The United Arab Emirates (U.A.E.) Foothills area has been less explored and constitutes a rather frontier area for petroleum exploration. Several questions still remain on the petroleum system (source rock, reservoirs and seals). Answers are required to minimize the exploration risks related to the recognition of potential small fields controlled by complex structural and stratigraphic traps. Previous seismic studies were based on conventional exploration seismic surveys. Due to the limited regional extent they can not clearly image the deepest sedimentary layers and the basement. In order to acquire continuous information along regional transects, from the surface to the base of the crust, deep seismic surveys across the Oman–U.A.E. Mountains penetrating down to 50 km below the surface of the earth were undertaken. This type of survey can assist in the understanding of the tectonic evolution throughout the geological ages and its impact on the present day structural features (Pinet and Bois 1990). The

general objectives of this study performed by several companies under the supervision of British Geological Survey are the thickness of the Semail ophiolite, outcropping in the eastern part of the peninsula, the study of the crustal architecture and of the thermal and burial history of potential source rocks and reservoirs (see [BGS website](#) address indicated in the references). The specific objective of the depth seismic imaging study performed by IFPEN is to determine the present day architecture of the frontal triangle zone to delineate deep subthrust prospects which are likely to extend farther east in the fold and thrust belt area.

Data Set

Four long listening seismic profiles have been recorded by Western Geco in the Northern Emirates for the Ministry of Energy of the United Arab Emirates: two profiles D1 and D4 from West to East, crossing by two shorter profiles D2 and D3 (from North to South) (Fig. 7.1) (Ministry of Energy 2007).

This deep seismic survey has been especially designed to provide new images of the deep geological structures in the compressive area and it has been implemented to cover the main domains through the Northern Emirates. The seismic recording parameters are characterized by a 40 km long split spread and 8 vibrators with a 20 s sweep (6–48 Hz) resulting in a large number of elementary traces of 20 s time length and sampled every 4 ms. Particularly, the profile D2 crosses the northernmost part of the Semail Ophiolite and the Dibba zone, just south of the Musandam Platform exposures. The study described in this paper is restricted to the processing and interpretation of the seismic profile D1. The different structural domains can be clearly identified all along the central part of the profile D1. Using well data, a schematic structural cross-section has been built (Fig. 7.2). From West to East, this deep seismic profile crosses two main geological domains. The late Cretaceous–Cenozoic foreland basin covers the western onshore province (low lands). The presence of relatively gentle dipping layers would ensure to obtain significant information about the thick carbonate platform of the former passive Arabian margin (from Permian to Middle Cretaceous) which could be a potential target for petroleum exploration. The late Cretaceous–Cenozoic fold and thrust belt extends over the eastern portion of the Emirates. In addition to the presence of compressive structures, the eastern part of the peninsula corresponds to the current elevated topography of the Oman Range where peridotite and serpentine of the Semail Ophiolite are exposed.

Two main compressional episodes account for the present architecture of the Northern Emirates. Firstly, a deformation initiated in the Late Cretaceous, resulting in the obduction of the Semail Ophiolite and in the progressive

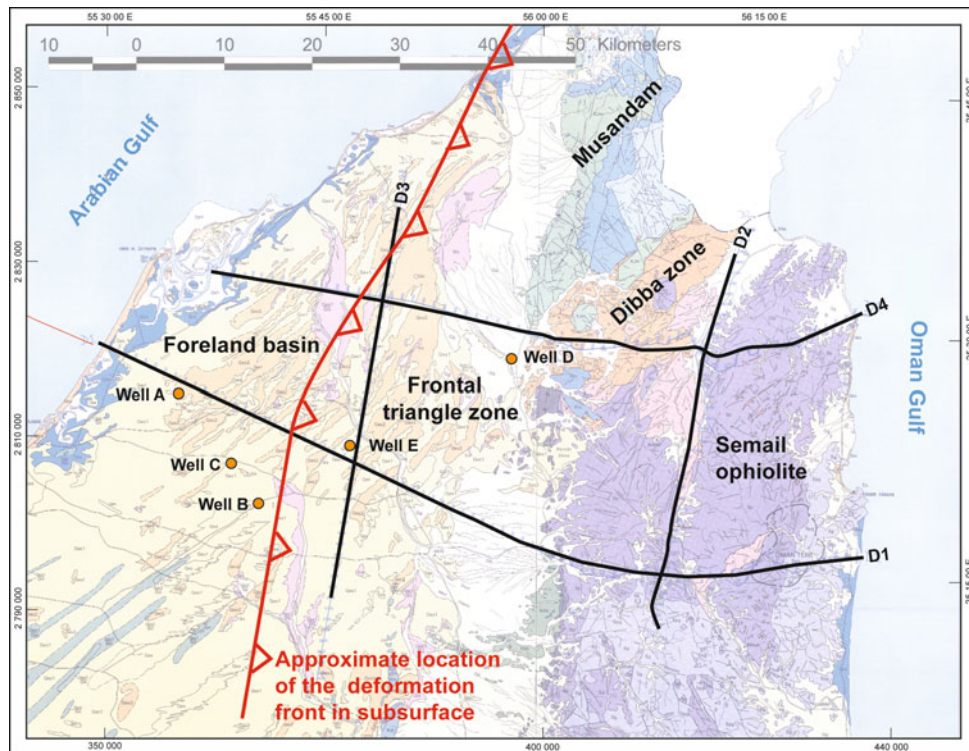


Fig. 7.1 Location map of the four deep profiles acquired across the Northern Emirates. The data used in this depth seismic imaging study are limited to the seismic profile D1 and to the wells located on this map

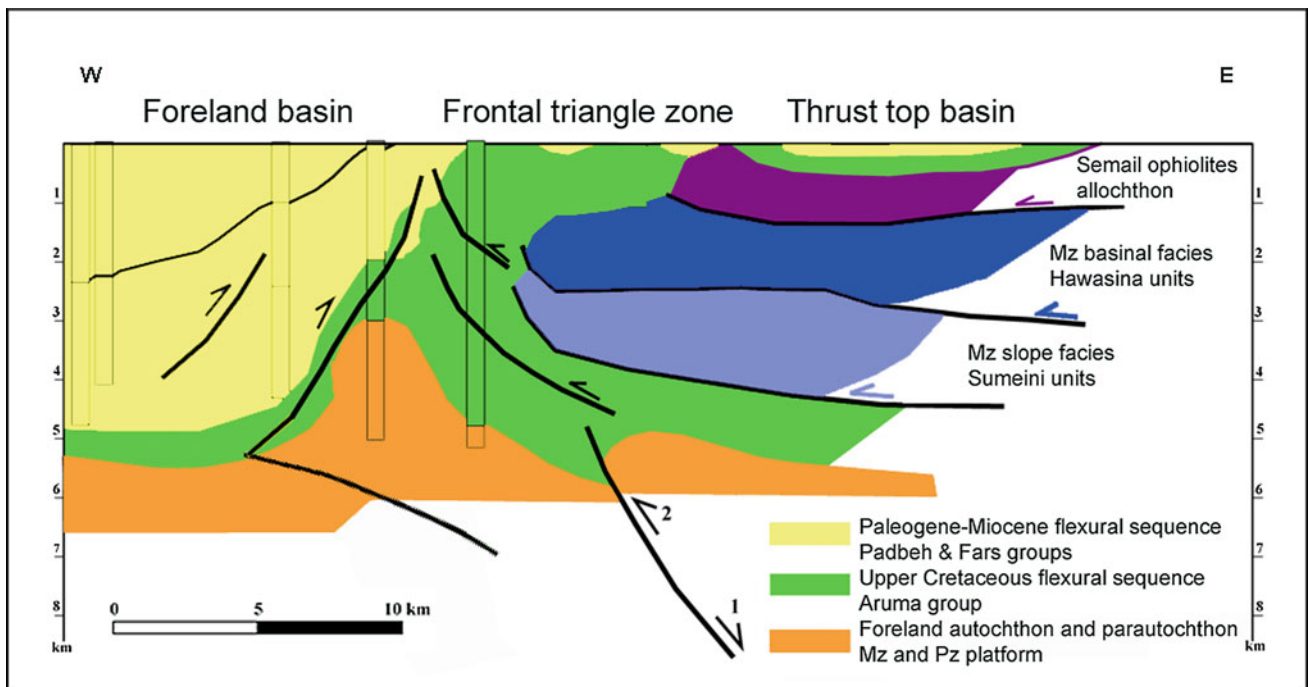


Fig. 7.2 Schematic depth structural cross-section across the Northern Emirates. This cross-section is built using well data in the vicinity of the profile D1 (modified from ministry of energy 2007)

accretion of the Hawasina and Sumeini tectonic wedge on top of the Arabian foreland, leading to a progressive bending of its lithosphere and development of a wide

flexural basin. Then, a compressive phase resumed during the Neogene, leading to the development of out-of-sequence thrusts and triangle zones, and refolding of the sole thrust of

the former Late Cretaceous accretion wedge (Tarapoa et al. 2010 and references herein).

A first velocity model is built using known velocity information: the velocity of the very near surface layers from uphole measurements, regularly spaced along the lines and with depths from 60 to 120 m and layer velocities from wells located in the vicinity of the profile D1. Velocities, depths or thicknesses from well data can be introduced as constraints for different formations during the tomographic inversion steps (Fig. 7.1). Only the well A is available near the western part of line D1, but the final depth is not deep enough to reach the carbonate platform, the target potential reservoir. Wells B and C are relatively far from line D1 and considering the strong lateral variation of velocity could not be trustfully used for velocity determination. Well D was the unique well near the central part of line D4, and drilled only the carbonate formations (limestone and dolomite) with velocities varying from 4,500 to 6,000 m/sec without reaching other formation underneath. Well E, located near the crossing of lines D1 and D3, has been logged with sonic and density tools. The Hawasina-Sumeini formation shows two different units, the velocity increasing strongly from 3,000 to 6,000 m/sec with depth. Velocity and depth data measured all along the well E is essential to constrain the tomographic inversion process, especially the strong lateral velocity variations in the Fars formation, the vertical velocity variations in the Hawasina-Sumeini formation and the depths of the main horizons around well location.

Reflection Tomography with Sand Dune on Surface in Western Foreland Area

When the near surface formations are sand dunes, the quality of the seismic time stack section is sufficiently good to give a reliable view of the subsurface structures (Fig. 7.3). In the western foreland area, the overburden is constituted by synorogenic series from the Padbeh Formation to the Upper Fars formation (from Paleogene to Miocene ages respectively). From the surface (−300 ms) down to the 4 s time line, clear seismic reflections underline a series of unconformities like erosional truncations and pinch-outs. A progressive eastward thickening of both the Lower and Upper Aruma in the autochthon is visible on the western part of line D1. Below these series, lies the carbonate platform identified by the strong amplitude reflections of the top Wasia (Hajar supergroup of Upper Cretaceous), slightly faulted by normal faults and dipping to the east, outlining the foreland regional flexure. The multi-offset reflection tomography has been applied using the following input parameters. Six different reflectors were selected taking into account both clearly identified unconformities and strong amplitude reflections: Upper Fars,

Lower Fars, Top Salt, Top Pabdeh, Top Aruma and Top Wasia. The reflection travel times are picked on partial stack sections; with a sequence of 100 m offset distance, from the nearest offset and up to offset 4,000 m when possible.

The structural complexity is too important to perform directly the global tomography inversion of all interfaces and all velocities. To stabilize the inversion algorithm, constraints on the velocity values and interface depths were imposed at the A well location. Thus, a layer stripping approach was firstly applied to estimate both lateral and vertical velocity variations and geometry of horizons. Then the results for each reflector—velocity variations and horizon geometry—were validated. As a good quality control criterion, histograms, cross-plots and RMS values of time residues obtained after each layer stripping inversion step are analyzed. After validation, the parameters computed by traveltime inversion were fixed and then the inversion of the next layer was performed. After achieving a suitable model with the layer stripping approach, a final inversion was performed, using the final model obtained by this approach as initial model. No major changes were observed, which indicates that the layer stripping approach did not introduce strong bias in the individual time event inversion. The global root mean square value (RMS) obtained is 4.9 ms, which indicates a very reliable inversion result. The Fig. 7.4 presents the location of the time residues for the deepest inverted reflected, top Wasia, and the associated computed velocity model (layer velocities and interfaces). Furthermore, as quality control, map of time residues and histograms, function of offset and CDP values are checked to validate the results obtained by the layer stripping approach for Top Wasia. Most of strong residues visible on control plots have been explained by interpretation errors, e.g. the eastern part of the Top Aruma. For Top Pabdeh, the relatively strong residues are due to the fact that the reflector is poorly illuminated with only 1000 m of maximum offset range (Fig. 7.5). The final model may be considered as a good model (Fig. 7.6). Both interfaces and velocities are acceptable from geological and geophysical point of view. Finally, the main fault identified on time stack section, has been introduced in the model but was not inverted because this event was not reached by a sufficient number of rays. The final evaluation of this result is obtained by control of reflected event flatness in trace gathers after the application of pre-stack depth migration and will be presented in the last chapter of this article.

Joint Reflection and First Arrival Tomography in the Central Frontal Active Area

In the central part of the line D1, the topography is usually rugged and is associated with near surface velocity

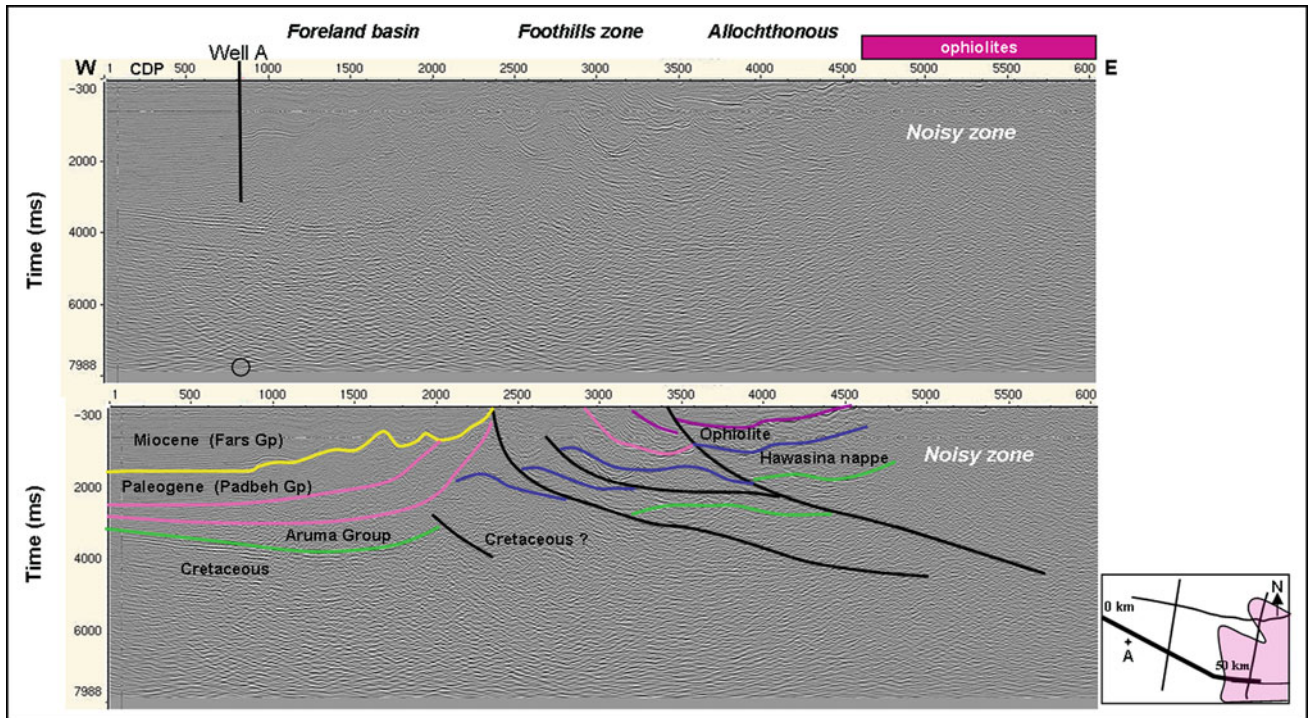


Fig. 7.3 Time migrated stack of the western part of profile D1 without and with seismic interpretation. The area where the ophiolite crops out, is indicated at the top of the seismic image

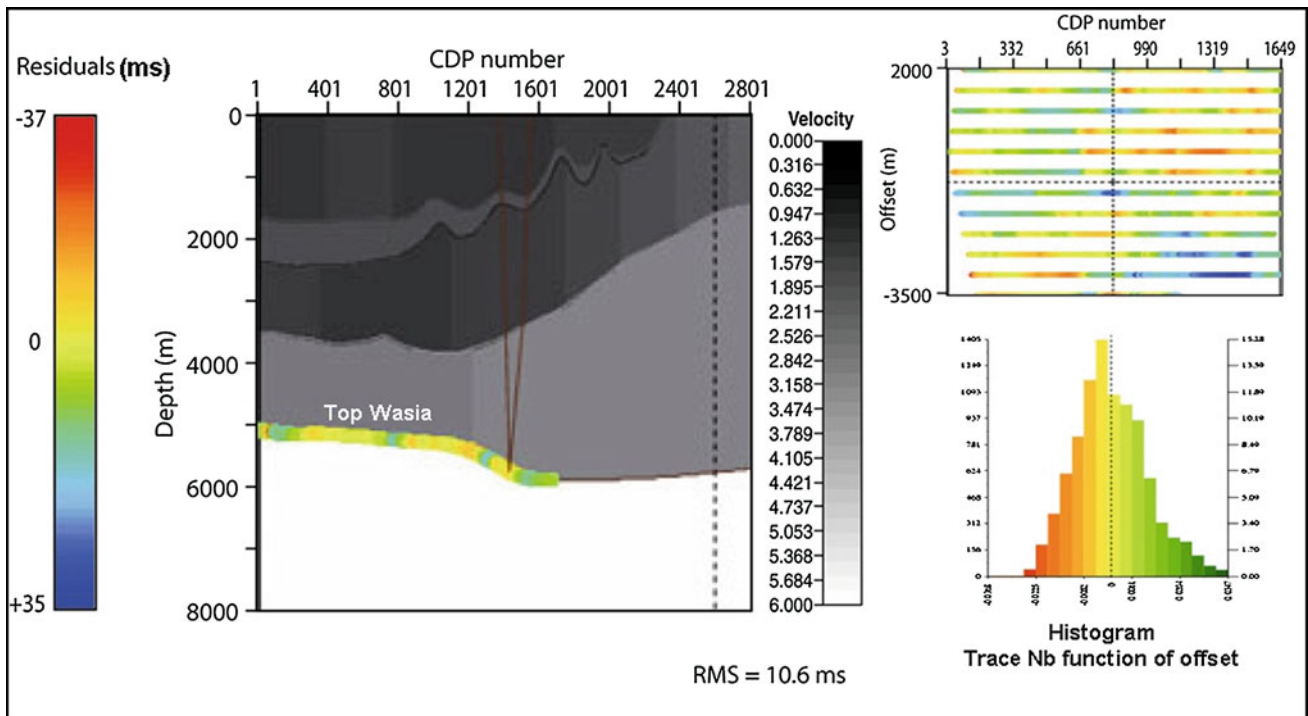


Fig. 7.4 Reflection tomographic inversion in the foreland (western part of D1): Inversion of Top Wasia (Upper Cretaceous). Velocity model is displayed with overlays of time residuals (differences between observed and synthetic times) along the reflector. Histogram (right bottom) and cross-plot (right top) are used to check the quality of tomography results as the RMS value is equal to 10.6 ms

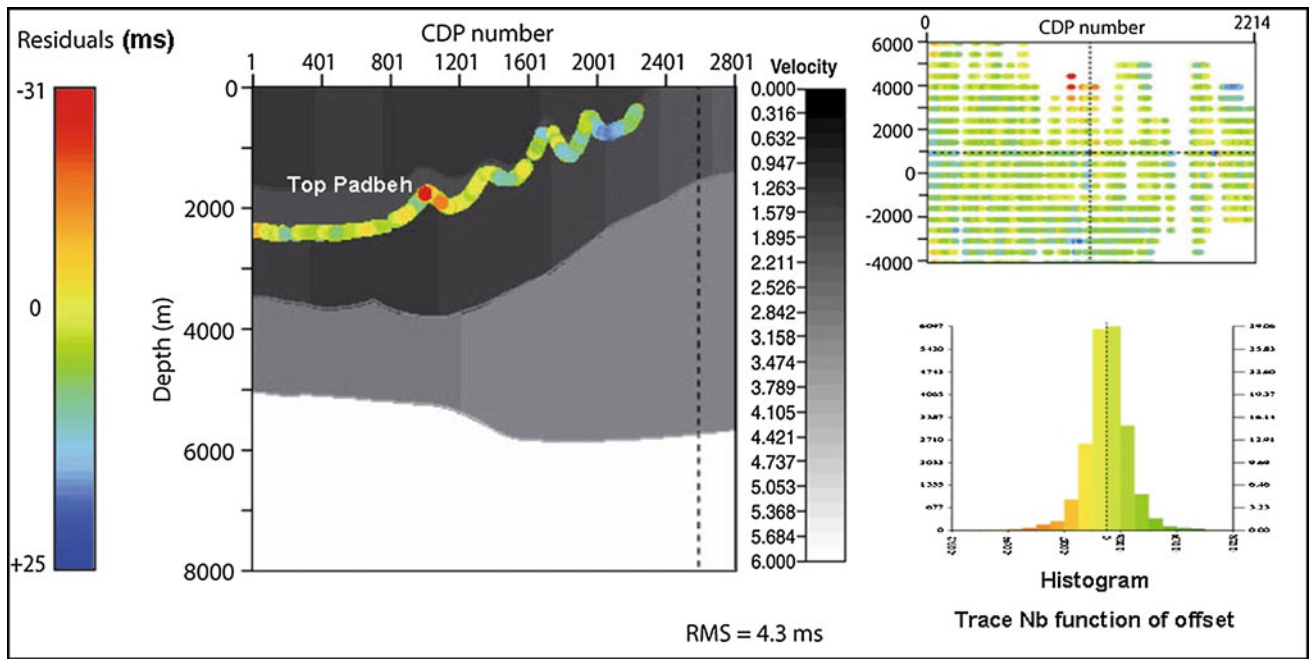


Fig. 7.5 Reflection tomographic inversion in the foreland (western part of D1): Inversion of Top Padbeh (Paleogene). Velocity model is displayed with overlays of time residuals (differences between observed and synthetic times) along the reflector. The residuals up

to 30 ms are due to the limited illumination of this relatively shallow reflector. Histogram (*right bottom*) and cross-plot (*right top*) are used to check the quality of tomography results as the RMS value which is equal to 4.3 ms

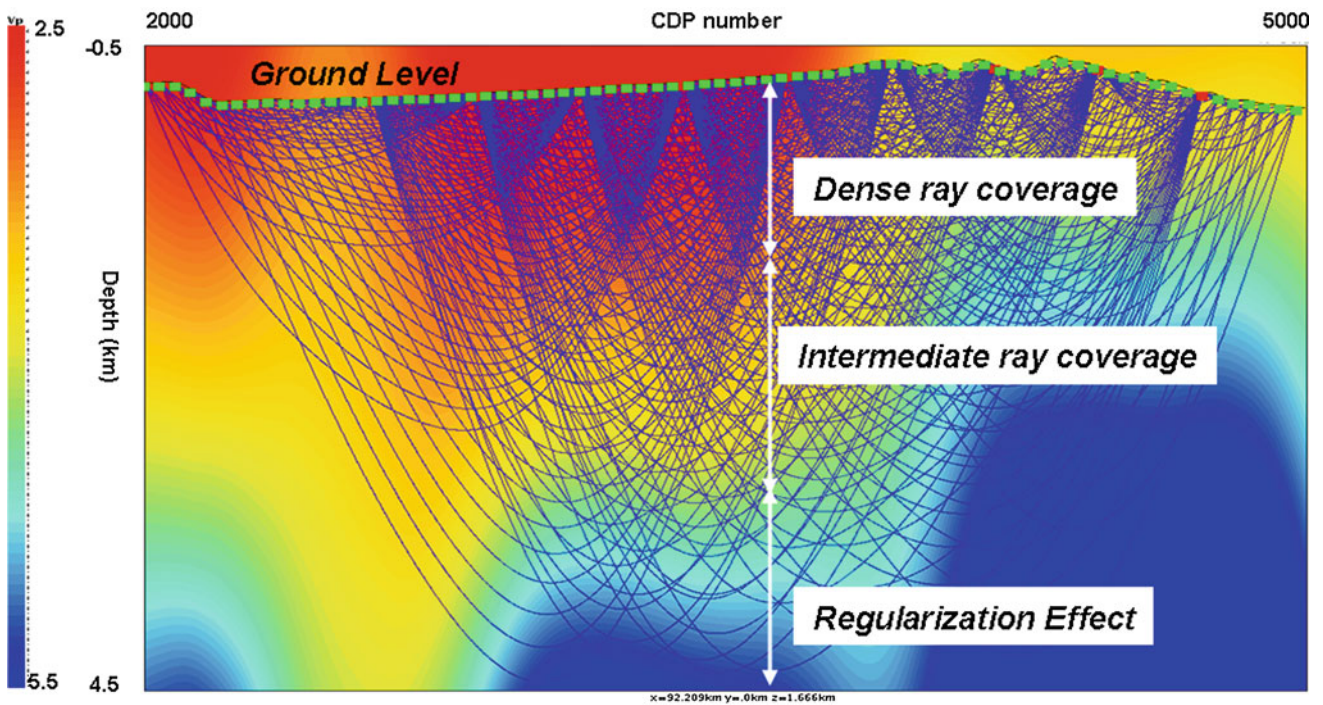


Fig. 7.6 Depth velocity model only determined by first arrival tomography in the foothills zone of the profile D1. Illumination of subsurface by diving waves is limited by the ray coverage computed by ray-tracing

inversions which degrade the quality of the seismic image. These characteristics lead to low signal-to-noise ratio, inadequate penetration of energy through overburden, poor geophone coupling with the surface and wave scattering. The quality of the time stack sections is deteriorated and seismic interpretation leads to bigger uncertainties in structural interpretation (Fig. 7.3). In the central part, the velocities are insufficiently determined by conventional velocity analysis to accurately convert the time sections into seismic depth images. The reflection tomography that was successfully applied in the foreland, partially failed in the foothills area, due to lack of continuous reflectors. Then a joint application of first arrival and reflection tomography has been performed to improve seismic imaging of major structural features by computation of a combined velocity model until the top Wasia (Upper Cretaceous). In our case study, regarding the availability of long offset data, we could reach deep layers (down to 2 km) using first arrival data, what could be very helpful in areas for which the picking of seismic reflections becomes very hard. The objective of the first arrival tomography is to build the velocity model in the upper part until 4 km. For first arrival tomography, the synthetic data are modelled as turning rays propagating in a smooth medium $v(x,y,z)$ and are calculated by the two point paraxial ray-tracing technique. An initial model is built using a priori velocity information and is valid if two conditions are satisfied. Firstly, the initial model tested with a given survey should have a sufficient number of captured rays or calculated travel times (Fig. 7.6). Secondly, the root mean square value of time residues (differences between observed and calculated travel times) should be less than 100 ms according to acquisition parameters. The picking of first breaks corresponding to first arrivals was done automatically up to 15 km offset (Fig. 7.7). But, over approximately 10 km offset, the accurate picking of the first breaks often become difficult due to the noise. At this step, we applied a first decimation of 1 shot out of 4 after application of a constant velocity correction of 3,000 m/s to facilitate the automatic picking. Using the time data base we performed an additional decimation both on the shots (1 shot/2) which led to a shot every 200 m and 137 shots) and on the traces (1 trace/5) which led to 1 trace every 125 m and 33,120 traces). A first inversion was carried out on the decimated dataset, and yielded to a first arrival velocity model after 12 iterations. The RMS value is 90 ms, which is relatively high but the misfits are compatible with the picking uncertainties related to low signal-to-noise ratio on raw data, especially for far offset traces. In order to improve the result, we manually improved the picking of the first arrival and performed a finer inversion in this part. The quality control shows some improvements: a better RMS value of 60 ms (which is still compatible with the new picked data noise) and globally a better match

between observed and calculated traveltimes. The deeper part of the velocity model is estimated by the joint inversion of the first arrival data and reflection data. Since the identification of deep events continued to be difficult, the reflectors interpreted by the geologist in the post-stack migrated time section were imported as a guide to pick the travel times on the other offset sections. The top Wasia, located in the central part of the line D1 was picked and inverted jointly with the first arrival data. The physical constraints on the velocity and depth values of this interface measured at A well are introduced to find a velocity model with very satisfying quality indicator, i.e. an RMS value equal to 20 ms, compared to the picking difficulties and the poor quality of the reflection data (Fig. 7.8). The velocity model obtained by this joint first arrival and reflection tomography has been merged with the reflection tomography velocity model of the western part to cover the whole line (Fig. 7.10). This model efficiently combines the improvements obtained by the two methods.

First Arrival Tomography in the Eastern Area Where the Semail Ophiolite Crops Out

On the eastern part of line D1, the presence at ground surface of the ophiolite unit, a very high velocity layer, generates the dispersion of the seismic waves and a very poor penetration of the seismic energy below this layer giving a very difficult interpretation (Fig. 7.1). The first arrival tomography already used in the central part of line D1 has been applied to build a velocity model in the eastern part of this line. The first arrival times were picked on raw shot point gathers after trace flattening with a constant velocity value: this value is 5,000 m/s for shot points acquired where the Tertiary formations outcrop and 7000 m/s for shot points acquired where the ophiolite formation outcrops (Fig. 7.9). The initial velocity model has constant horizontal variations and a constant vertical gradient. The topography is introduced in the inversion software because variations of at least 400 m are important and must be modelled for synthetic travel times computation and for better evaluation of the near surface velocity layers. The velocity model has been computed taken into account firstly the offset range of $\pm 8,000$ m and completed in the deeper part (below 2 km) by introducing the first arrival picked times from 8 to 15 km offset traces. The ophiolite layer outcropping at ground level could be correlated with a velocity increase (from 3 to 4.5 km/s). The isovelocity line of 5.5 km/s could indicate the top of the high velocity layer below the ophiolite layer. This result is consistent with the refraction feasibility studies performed on line D1 and D4 estimating a 6 km/s velocity value for the base of the ophiolites (Naville et al. 2010 and this volume). This velocity model estimated for the eastern part of line D1

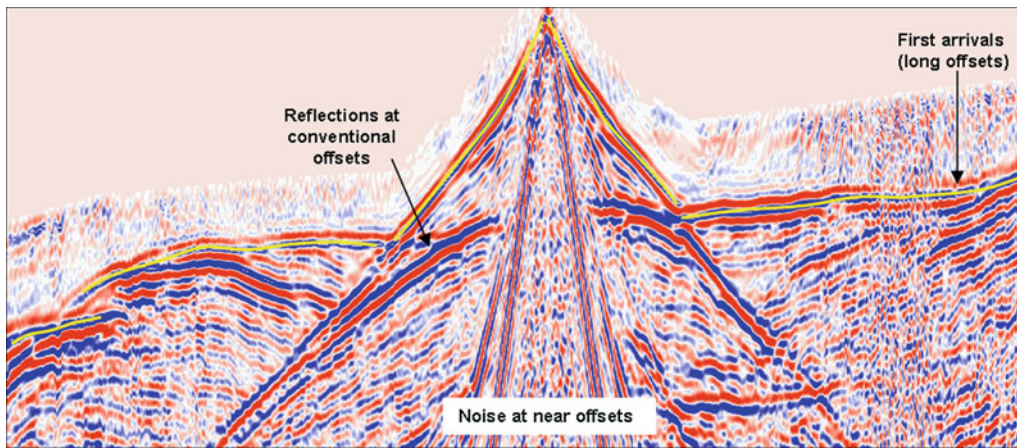


Fig. 7.7 First arrival tomography in foothills zone. Example of a raw shot point in the central part of the line D1 with automatic first arrival picking after a constant velocity correction of 3,000 m/s

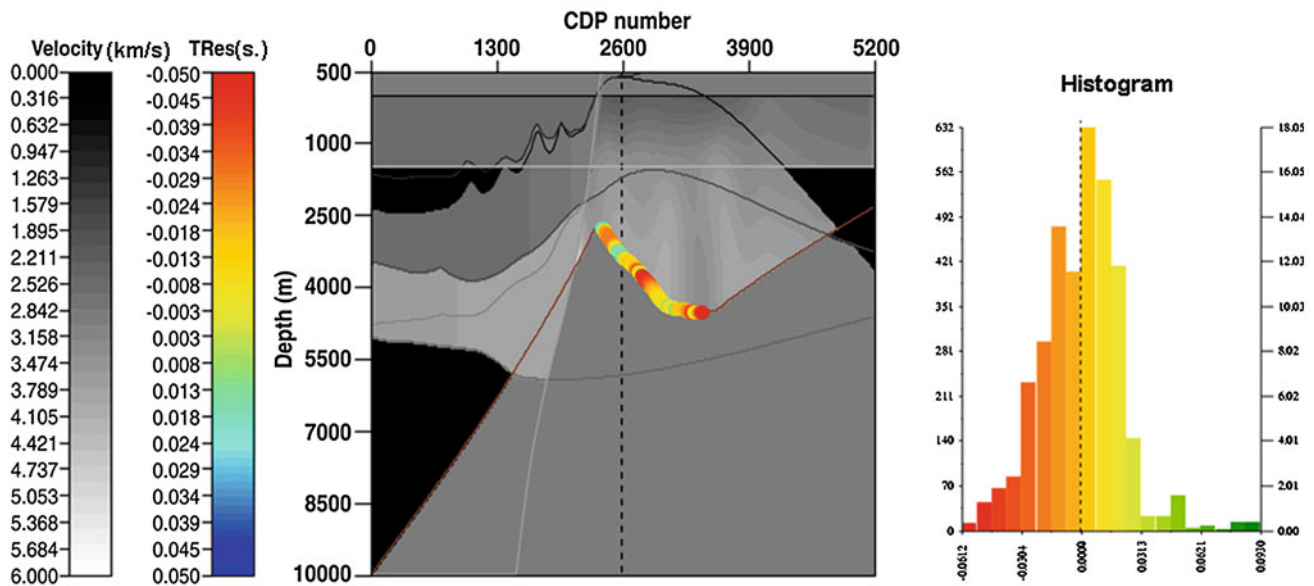


Fig. 7.8 Results of joint first arrival and reflection tomographic inversion in the foothills zone. In the central part of the profile D1 (from CDP 2200 to 4800), the depth velocity model above Top Wasia

is computed using simultaneously first arrivals and reflected travel-times. The RMS value is equal to 20 ms

is combined with the velocity models of the western and central parts to build the complete velocity model presented on Fig. 7.10.

Tomography Evaluation Using Depth Seismic Migration

Pre-stack Depth Migration

Pre-stack depth migration processing was carried out using the velocity model computed by reflection and first arrival tomography. According to the frequency bandpass of input

data, pre-stack depth migration was carried out with the limited 45 Hz low pass filter and with 45° aperture. Two migrated stacks were computed, respectively with a maximum offset of 4 and 8 km. The image obtained with longer offsets of 8 km is better especially in the central deep part, where some reflectors appear more clearly. Common image gathers were computed each 12.5 m (equal to the CDP interval distance). On the western and central parts of the line D1 (from CDP 1 to CDP 4400) most of the traces gathered in common reflector point show flattened events ensuring a good quality control for both velocity model and depth image (Fig. 7.11). Then, post migration processing including amplitude equalization and random noise filtering

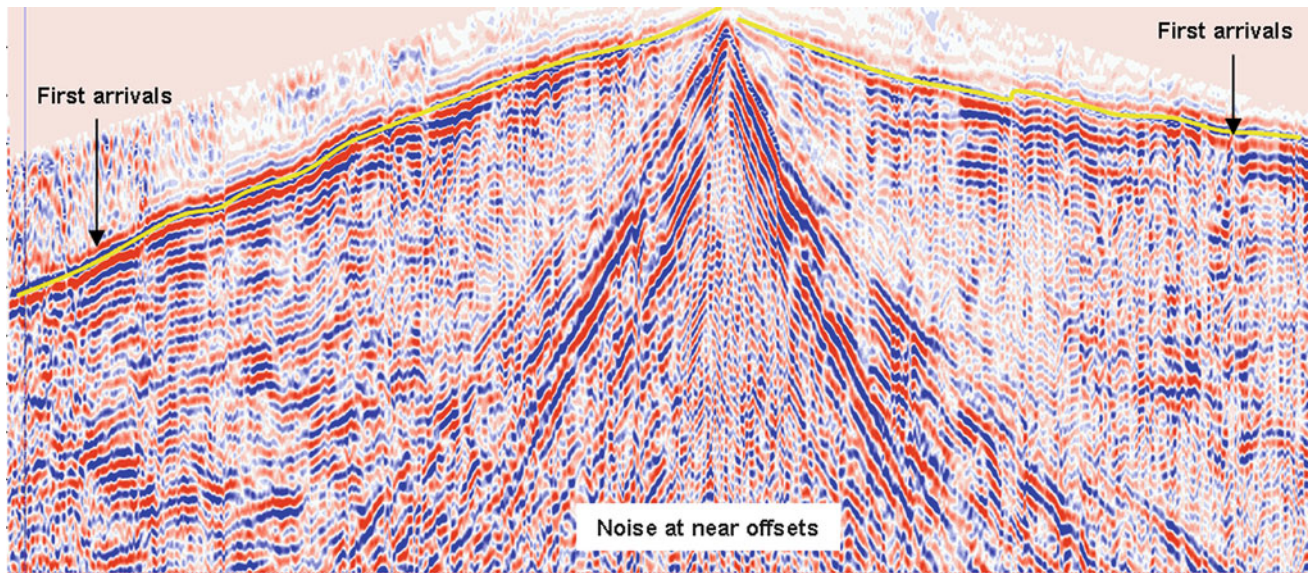


Fig. 7.9 First arrival tomography in the area where the Semail ophiolite crops out. Example of a raw shot point in the eastern part of line D1 W with automatic first arrival picking after a constant velocity correction of 7,000 m/s

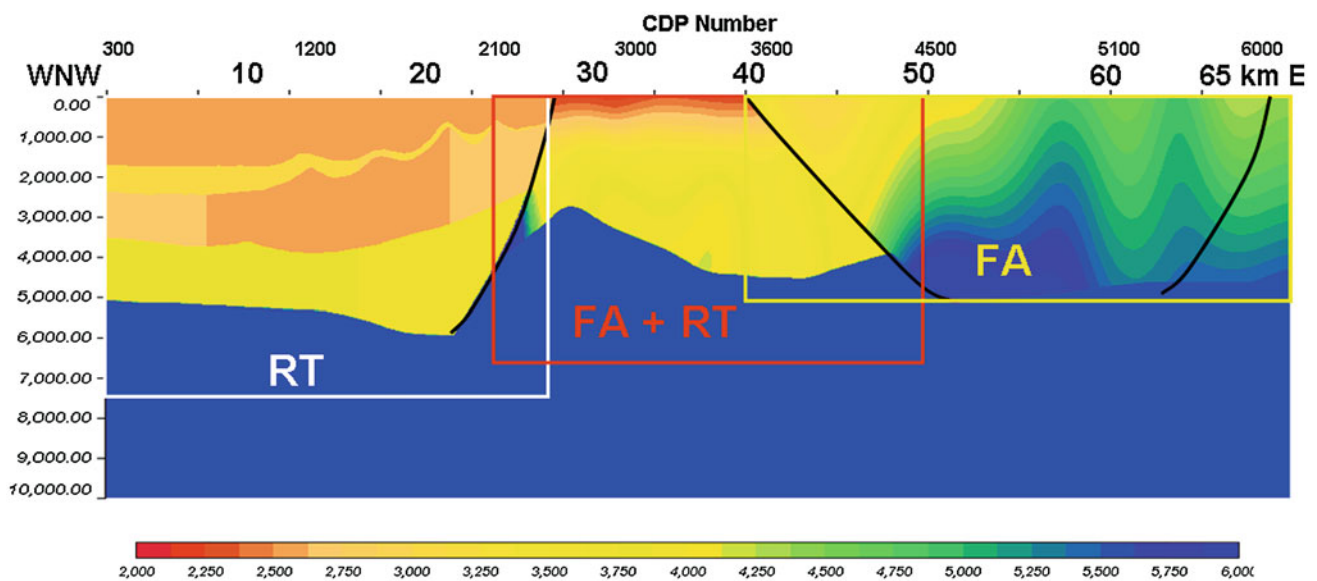


Fig. 7.10 Final depth velocity model along the profile D1. This model was computed by reflection tomography (*RT*) in the western part (foreland), joint reflection and first arrival tomography

(*FA + RT*) in the central part (foothills) and first arrival tomography (*FA*) in the eastern part (ophiolite outcrop). Two velocity *contrast lines* in *black* indicate the limits between the different tectonic domains

was carried out to obtain the best depth migrated images at target interfaces (Fig. 7.12). But, in the eastern part where the ophiolite crops out (East of CDP 4400), the quality of the depth migrated image is not sufficiently good to improve the interpretation. This is probably due to very low signal remaining below the ophiolite overburden which has distorted and attenuated the seismic energy. Better seismic images have been obtained with a specific time processing integrating the results of the refraction study (Neville et al. 2010 and this volume).

Depth Structural Interpretation

Interpretation of this final depth seismic image was then confidently performed to obtain new information about the structures recognized along this profile (Fig. 7.12). In the western foreland, the depth and the structural features of the carbonate platform top (Upper Cretaceous) that was not reached by any well is now estimated with more confidence along this part of the profile. In the central foothills part of the profile, and to the timing of structural closures of

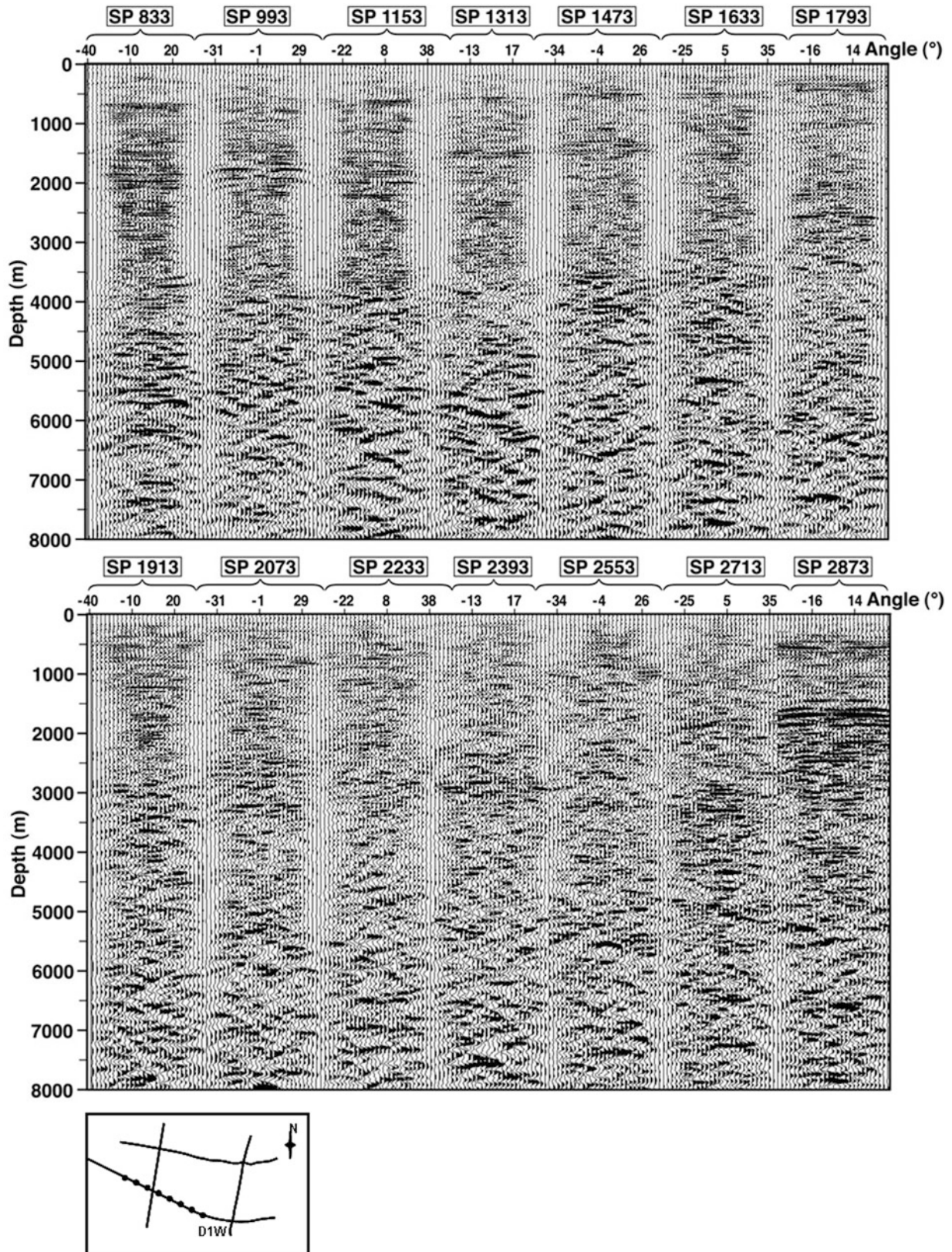


Fig. 7.11 Selection of common depth point gathers. These gathers, indicated in SP position, are selected along the central part of the profile D1 (foothills zone). When these seismic events are nearly flat,

the time to depth conversion is good because all the traces of the same gather illuminate the same subsurface point

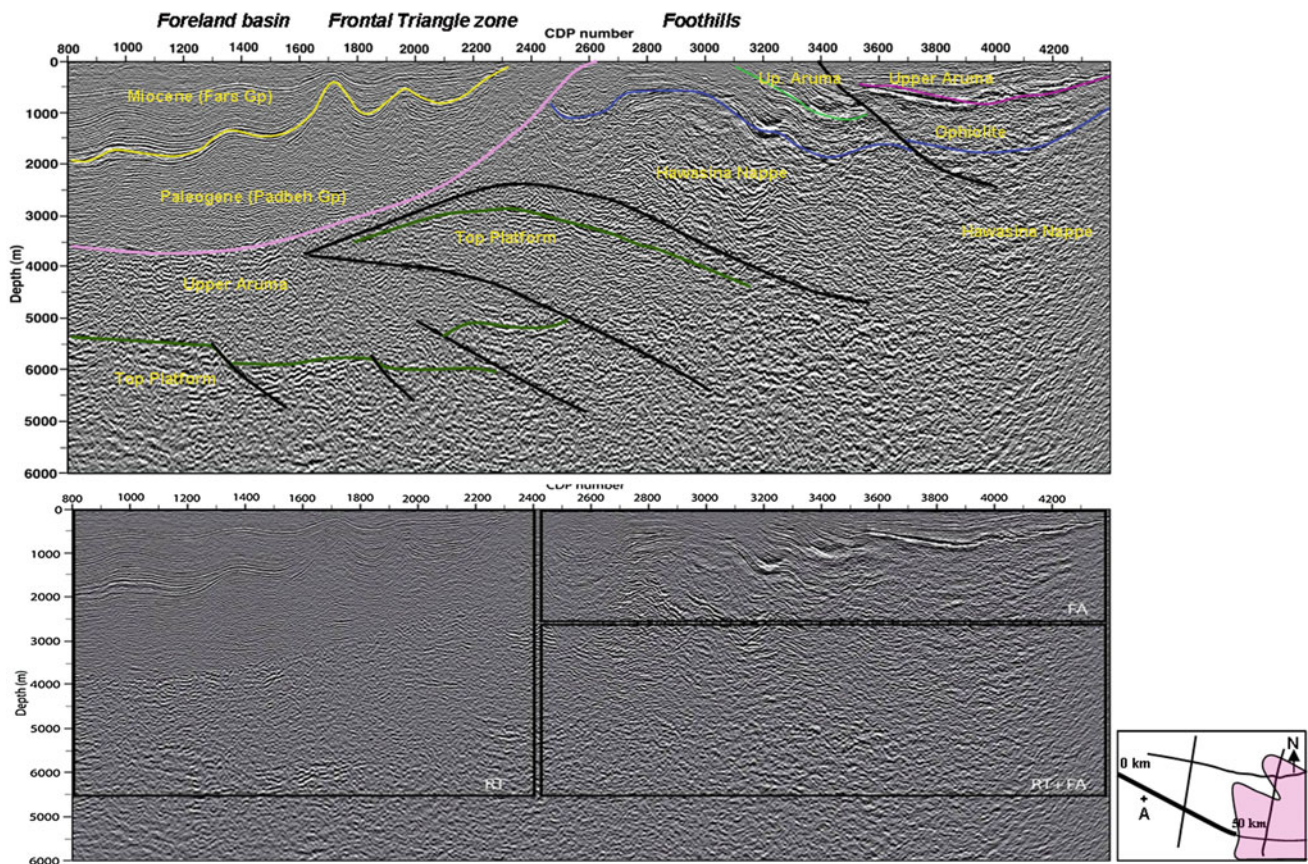


Fig. 7.12 Final depth migrated image. The seismic interpretation is directly done on the depth migrated profile D1 in the foreland and foothills zones (*top image*). The uninterpreted depth image obtained

after stacking of migrated traces from the nearest offset up to offset 8 km is displayed on the *bottom* of this figure

potential traps. Available conventional seismic linesthe major decoupling occurring between the far travelled Hawasina nappes and the underlying platform carbonate units is more accurately identified.

A cross-section has been built integrating all the data (geology, seismic, well, velocity) from now on available in the depth domain (Fig. 7.13) (Tarapoanca et al. 2010 and this volume). In the eastern region where the ophiolite crops out, the limits between the Semail ophiolite, the high velocity layer and the Hawasina nappes that were obtained by first arrival tomography and refraction studies were now introduced in this model (Neville et al. 2010 and this volume). A cross-section balancing technique (unfolding) was applied to this structural model, in order to check the overall consistency of the interpretations (length and thickness of the various sedimentary units, lateral and vertical offsets along the main faults). That also results in more realistic restored geometries of the profile. Using this present day model, a kinematic modelling was carried out to retrieve the initial and final geometry of the main formations along the cross-section and also to perform a petroleum system evaluation (Tarapoanca et al. 2010, and this volume).

Conclusion

We have presented the application of the traveltime tomography method developed by IFPEN for velocity model estimation and depth imaging. Because this traveltime inversion algorithm is very flexible, a joint tomography process of several seismic events (e.g. primary reflections and first arrivals) can be performed in a single run. Furthermore regarding the geological complexity, any type of depth or velocity constraints from well data and regional geology, could be easily taken into account. Application of this traveltime inversion on a deep seismic profile acquired across the Northern Emirates Foothills has shown the benefits of combining reflection and first arrival tomography to overcome the difficulties of each particular method. The final velocity model was used to migrate in depth the long offset seismic gather and obtain a new depth migrated image across the peninsula.

In the western foreland, strong lateral velocity variations are mainly generated by stratigraphical variations inside slightly dipping layers. In this case, reflection tomography

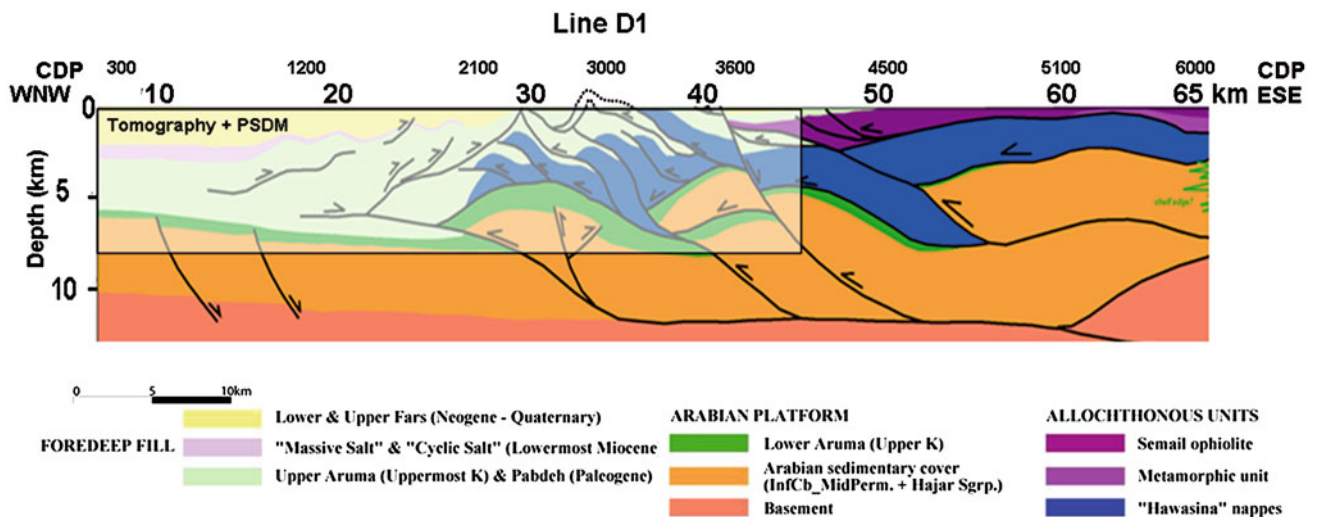


Fig. 7.13 Cross-section along a part of the profile D1. The *white rectangle* shows the domain over which tomographic inversion followed by depth migration were applied. This cross-section

integrates geological and depth seismic studies (see for more details on geological study: Tarapaonca et al. 2010 and Naville et al. 2010 and this volume)

gives reliable velocity models because continuous reflections could be easily picked and the reflections were slightly distorted by the velocity contrasts. Then, the depth migrated seismic image has been improved leading to more confident evaluation of the structural feature of the deep carbonate platform, the potential reservoir.

In the central part of the profile, the overburden becomes more complex with steeply dipping or even vertical layers. In this foothills zone, using traveltimes inversion of very far offset traces up to 15 km has allowed to combine shallow seismic events deeply illuminated by diving waves and reflected energy generated by deeper reflectors. We have shown that the joint application of reflection and first arrival tomography has provided a more complete velocity model. After pre-stack depth migration, an improved depth seismic image has been computed and a more reliable structural interpretation of the complex triangle zone of the line D1 has been performed directly in the depth domain.

In the eastern part of the line D1, the outcrops are made up of the Semail ophiolite; a very high velocity layer. The velocity model describing the large vertical and horizontal velocity variations of this overburden has been well determined using first arrival tomography. Nevertheless, the quality of the depth migrated seismic image was not really improved and remains very noisy and difficult to be confidently interpreted. This is due to the very complex propagation and the limited energy penetration through the screen generated by the ophiolite formation.

Finally, we would like to emphasize that the quality of these depth migrated images and the reliability of the velocity models computed by tomography were due to the availability of very long offset seismic traces deeply illuminating

interfaces by first arrivals and reflected waves. This is a good example of the contribution of this type of seismic survey for petroleum system evaluation in underexplored complex area.

Acknowledgments We acknowledge MM Saleh Al Mahmoudi, Khalid Al Hosani, Abdullah Gahnoog and the Ministry of Energy of the UAE for their long-term support during this project and for authorizing this publication. We also thank Louis Chérel from IFP Energies nouvelles and Daniela Justiniano, former trainee from IFP-school, for their contribution to tomography and depth migration. We thank the anonymous reviewer and Charles Naville for their reviews of the manuscript and their very useful comments about the traveltimes tomography and the case study presentations respectively.

References

- Bêche M, Kirkwood D, Jardin A, Roue F (2005) 2D Depth seismic imaging in the Gaspé Belt, a structurally complex fold and thrust belt in the Northern Appalachians, Québec. Springer, Canada, pp 75–90
- Bêche M (2009) Architecture structurale de la ceinture de Gaspé (Canada): imagerie sismique intégrée et application à l'évaluation pétrolière, Ph D thesis University of Cergy-Pontoise, France and University Laval, Canada
- Bishop TN, Bube KP, Cutler RT, Langan RT, Love PL, Resnick JR, Shuey JT, Spindler DA, Wyld HW (1985) Tomographic determination of velocity and depth in laterally-varying media. *Geophysics* 50:903–923
- Bloor R (1998) Tomography and depth imaging. 60th EAGE Conference and Exhibition, Expanded Abstracts, 1–01
- British Geological Survey web site on: <http://www.bgs.ac.uk/research/international/uae.html>
- Broto K, Ehinger A (1998) How to access 3D prestack kinematic information in case of complex geologies? 68th Annual International Mtg, Society of Exploration Geophysicists, Expanded Abstracts

- Broto K (1999) Accès à l'information cinématique pour la détermination du modèle de vitesse par tomographie de réflexion 3D: Ph.D thesis, University of Pau, France
- Broto K, Lailly P (2001) Towards the tomographic inversion of prismatic reflections. 71st Annual International Mtg, Society of Exploration Geophysicists, Expanded Abstracts
- Broto K, Ehinger A, Kommedal J, Folstad P (2003) Anisotropic traveltome tomography for depth consistent imaging of PP and PS data. *The Leading Edge*, February 2003, 22:114–119
- Broto K, Rakotoarisoa H, Nicoletis L (2008) Method of determining specular information after prestack seismic imaging. US Patent 7345951
- Broto K, Ricarte P, Jurado F, Le Bras C, Etienne G (2011) Improving seismic monitoring by 4D joint prestack traveltome tomography—application to the Sleipner CO₂ storage case. EAGE SES Conference, Valencia, Spain
- Clarke RA (1997) Modeling and inversion of 3D complex cinematic data, Ph.D thesis, University of Pau, France
- Delbos F, Gilbert JC, Glowinski R, Sinoquet D (2006) Constrained optimization in seismic reflection tomography: a Gauss–Newton augmented lagrangian approach. *Geophys J Int* 164(3):670–684
- Dell'Aversana P, Colombo D, Buia M, Morandi S (2003) Velocity/interface model building in thrust belt by tomographic inversion of global offset seismic data. *Geophys Prospect* 51:23–35
- Delprat-Jannaud F, Lailly P (1993) Ill posed and well posed formulations of the reflection tomography problem. *J Geophys Res* 98:6589–6605
- Ehinger A, Broto K, Jardin A (2001) 3D tomographic velocity model determination for two North Sea case studies, 63rd Conference and Technical Exhibition, EAGE Amsterdam, Expanded Abstract Book
- Gray, S., Cheadle, S., and Law, B., 2000, Depth model building by interactive manual tomography: 70th Annual International Mtg, Society of Exploration Geophysicists, 914–917
- Gray S, Cheadle S, Vestrum R, Gittins J, Zhu T, Nanan H (2002) Using advanced seismic imaging tools to see the invisible beneath foothills structures. *CSEG Recorder*, March, pp 16–28
- Grau G, Lailly P (1993) Sequential migration-aided reflection tomography: an approach to the imaging of complex structures. *J Appl Geophys* 30:75–97
- Jardin A, Chaker R, Krzywiec P (2005) Understanding seismic propagation through triangle zones. In: *Thrusts Belts and Foreland Basins*, Lacombe, Lavé, Roure, Vergès (eds). Springer, pp. 63–74
- Jaiswal P, Zelt CA (2008) Unified imaging of multi-channel seismic data: combining traveltome inversion and prestack depth migration. *Geophysics* 73(5):269–280
- Jurado F, Sinoquet D, Ehinger A (1996) 3D reflection tomography designed for complex structures, 66th Annual International Mtg, Society of Exploration Geophysicists, Expanded Abstract
- Lailly P, Sinoquet D (1996) Smooth velocity models in reflection tomography for imaging complex geological structures. *Geophys J Int* 124:349–362
- Ministry of Energy, UAE (2007) Reports on deep seismic survey, 3 volumes
- Naville C, Ancel M, Andriessen P, Ricarte P, Roure F (2010) New constrains on the thickness of the Semail ophiolite in the Northern Emirates. *Arab J Geosci* 3:459–475
- Plaza-Faverola A, Westbrook GK, Ker S, Exley RJK, Gailler A, Minshull TA, Broto K (2010) Evidence from 3D seismic tomography for accumulation of gas hydrate. *JGR Solid Earth*, 2010
- Pinet B, Bois C (1990) The potential of deep seismic profiling for hydrocarbon exploration. Editions TECHNIP, Paris
- Renard F, Lailly P (1999) Robust and accurate determination of complex velocity/depth models by reflection traveltome tomography: KIM 1999 annual report. Institut Français du Pétrole, Rueil, France
- Stork C (1992) Reflection tomography in the postmigrated domain. *Geophysics* 57:680–692
- Tarantola A (1987) Inverse problem theory: methods for data fitting and model parameter estimation. Elsevier Science Publishers, Amsterdam, The Netherlands
- Tarapoanca M, Andriessen P, Broto K, Chérel L, Ellouz-Zimmermann N, Faure JL, Jardin A, Naville C, Roure F (2010) Forward kinematic modelling of a regional transect in the Northern Emirates using geological and apatite fission track age constraints on paleo-burial history. *Arab J Geosci* 3:395–411
- Versteeg R (1994) The Marmousi experience: velocity model determination on a synthetic complex data set. *Lead Edge*, September 1994, 927–936
- Zelt CA, Barton PJ (1998) Three-dimensional seismic refraction tomography: a comparison of two methods applied to data from the Faeroe Basin. *J Geophys Res—Solid Earth* 103:1292–1308
- Zhu T, Cheadle S, Petrella A, Gray S (2000) First-arrival tomography: method and application. 70th Annual International Mtg, Society of Exploration Geophysicists, Expanded Abstracts, 2028–2031
- Zhu X, Valasek P, Roy B, Shaw S, Howell J, Whitney S, Whitmore ND, Anno P (2008) Recent applications of turning-ray tomography. *Geophysics* 73(5):243–254